Efficient Global Sensitivity Analysis of Structural Vibration for a Nuclear Reactor System Subject to Nonstationary Loading

Gregory A. Banyay
University of Pittsburgh, Westinghouse Electric Company
Pittsburgh, PA USA
banyayga@westinghouse.com

Michael D. Shields
Johns Hopkins University
Baltimore, MD USA

John C. Brigham
Durham University, University of Pittsburgh
Durham, UK

Abstract

The structures associated with the nuclear steam supply system (NSSS) of a pressurized water reactor (PWR) include significant epistemic and aleatory uncertainties in the physical parameters, while also being subject to various non-stationary stochastic loading conditions over the life of a nuclear power plant. To understand the influence of these uncertainties on nuclear reactor systems, sensitivity analysis must be performed. This work evaluates computational design of experiment strategies, which execute a nuclear reactor equipment system finite element model to train and verify Gaussian Process (GP) surrogate models. The surrogate models are then used to perform both global and local sensitivity analyses. The significance of the sensitivity analysis for efficient modeling and simulation of nuclear reactor stochastic dynamics is discussed.

Introduction

Uncertainty pervades engineering processes for nuclear plants, which span across many disciplines from probabilistic risk assessment (PRA) and safety analysis, to up-front component design for a new plant (i.e., forcing function development, sub-scale and start-up testing), the aging management of operating plants (i.e., stress corrosion cracking, fracture mechanics, and non-destructive examinations (NDE)), and the design of fuel (i.e., core loading pattern optimization, departure from nucleate boiling (DNB) correlations). Furthermore, the contribution of uncertainties in design parameters to key outputs of interest is largely unknown in the early stages of design. Key outputs may include anything from stress intensities necessary to satisfy allowable limits (1) to component reliabilities that directly influence core damage frequencies determined in PRA (2), (3).

The lack of knowledge relating design parameter uncertainty to outputs of interest causes the design process to iterate many times; increasing time, effort, and cost. An inefficient design process may force constructors to begin construction prior to final design of all systems in a nuclear plant, further driving up cost due to in-field design changes. For an operating plant, lack of understanding of parameters can greatly increase maintenance costs. Uncertainty quantification (UQ) in the concept design is necessary to inform parameter sensitivities. Neglecting UQ can lead to overdesigned components and excessive maintenance and qualification expenses. Furthermore, commercial pressures within the power generation industry are driving engineering organizations to challenge the status quo and develop creative ways to keep nuclear

energy cost effective and safe. UQ and sensitivity analysis are necessary first steps toward applying computational mechanical analysis of system finite element models (SFEMs) for design optimization in the nuclear industry.

The contribution of parameter uncertainties must be quantified and adopted into design (and companion aging management) processes through sensitivity analysis. Specifically, global sensitivity analysis (GSA) applied to stochastic dynamic models of nuclear reactor structures provides measures of relative importance amongst multiple system/loading parameters to outputs of interest. If the influence of parameter uncertainties can be properly understood early in the engineering analysis, then the (intertwined) design, analysis, construction, operations, and maintenance processes may become more parsimonious.

Variance-based GSA, such as described in (4), (5), (6), and (7), requires running a model a large number of times (8). It is therefore of interest to either reduce the number of full-order runs (i.e., SFEM realizations) required to characterize sensitivity, or to replace the full-order model with a surrogate model that runs with minimal computational expense yet captures the relevant trends in the model performance. In recent years, reduced-order modeling techniques (e.g. (9), (10)) and surrogate modeling methods (e.g., (11)) have gained popularity for random vibration problems. Furthermore, several works have already applied surrogate models for sensitivity analysis, successfully reducing the computational expense significantly such as (12), (13), (14). Specific to the nuclear industry, (15) explored surrogate modeling and GSA for evaluating an upper internals assembly subjected to stationary flow-induced vibration

(FIV), and demonstrated the improvements offered by advanced sampling strategies including Latin Hypercube Sampling (LHS) and Latinized Partially Stratified Sampling (LPSS).

Various transient scenarios for which a nuclear plant must be designed are non-stationary random processes, having time-varying stochastic nature, such as a loss of coolant accident (LOCA) or an earthquake. Engineering simulations of such events often constitute a large computational expense, imposing a large financial impact on engineering design, operations, and maintenance. LOCA and seismic simulations can often govern the selection and placement of replacement components (e.g., baffle-former bolts) and also directly impact evaluations of nuclear power plant safety. Therefore, evaluation of methods which permit more credible engineering assessments, such as permitted by GSA, as well as methods which promote computational efficiency, such as surrogate modeling, focused upon non-stationary events are of distinct interest to the nuclear industry. Thus, a rigorous method requiring relatively few evaluations of full-order models is of paramount importance towards enhancing credibility, ensuring safety, and decreasing costs of modeling and simulation of nuclear reactor stochastic dynamics.

This paper presents the application of surrogate modeling and GSA methods to non-stationary stochastic dynamic finite element analysis of a reactor system subject to a LOCA scenario. SFEMs are used ubiquitously throughout the design and analysis of key systems, structures, and components within pressurized water reactors (PWRs) across the commercial nuclear industry, per (16), (17) and (18), for example. Despite

the centrality of SFEMs to the general mechanical and civil design of such high-consequence facilities, UQ for such computational models is generally lacking amongst nuclear industry practitioners. As such, this work builds upon that of (19) and (15) by considering a non-linear finite element model with multiple outputs, additional input parameters, and non-stationary loading. In the following section, the methodology is described including the manner in which non-stationary random vibration was simulated using finite element analysis, the Fourier Amplitude Sensitivity Test (FAST) used to accomplish the GSA, Gaussian Process surrogate modeling, and then the design of experiment sampling strategies employed herein. Then, the finite element analysis is described followed by the GSA results and companion discussion.

Methodology

Flow within a nuclear reactor coolant system is highly turbulent. The high turbulence is necessary for core cooling and heat transfer, but also creates substantial vibratory forcing on the associated mechanical components and assemblies. For analysis of reactor internals, M.K. Au-Yang developed methods for determining forcing functions in a downcomer annulus (20), modeling random vibration induced by turbulent flow (21), and summarized the majority of his published work in (22). Guidelines for practice are based on these works and others for dynamic analysis of nuclear components subjected to flow-induced vibrations (1). Recent industry efforts, such as (23), have sought to improve the methods described in (1). The aim of this work is to continue to improve methods of dynamic analysis for reactor structures.

The structural systems evaluated within this work involve random vibration due to non-stationary excitation, and the objective is to compute sensitivities for key parameters and outputs within these systems. To calculate the sensitivities in a computationally efficient manner, surrogate models are used in place of a full-order model (i.e., SFEM). However, to construct surrogate models, it is first necessary to efficiently sample the parameter values at which the SFEM will be evaluated to train the surrogate models. The methodology for simulating non-stationary random vibration, global sensitivity analysis, surrogate modeling, and sampling are presented in the following subsections.

FULL-ORDER NON-STATIONARY RANDOM VIBRATION ANALYSIS

Figure 1 and Figure 2 show a typical PWR and an associated SFEM, respectively. Recognizing that finite element models for advanced reactor applications possess hundreds of thousands of degrees of freedom, the finite element model chosen herein to simulate an operating PWR includes approximately 3,000 degrees of freedom consisting of various element types (e.g., beam, shell, spring, damper, etc.). Due to non-linearities in the SFEM response (16), such as displacement-dependent spring constants, and the non-stationary loading conditions associated with loss of coolant accident (LOCA) and seismic events (required by nuclear design analysis), the SFEM is executed using a dynamic transient finite element analysis with implicit time integration.

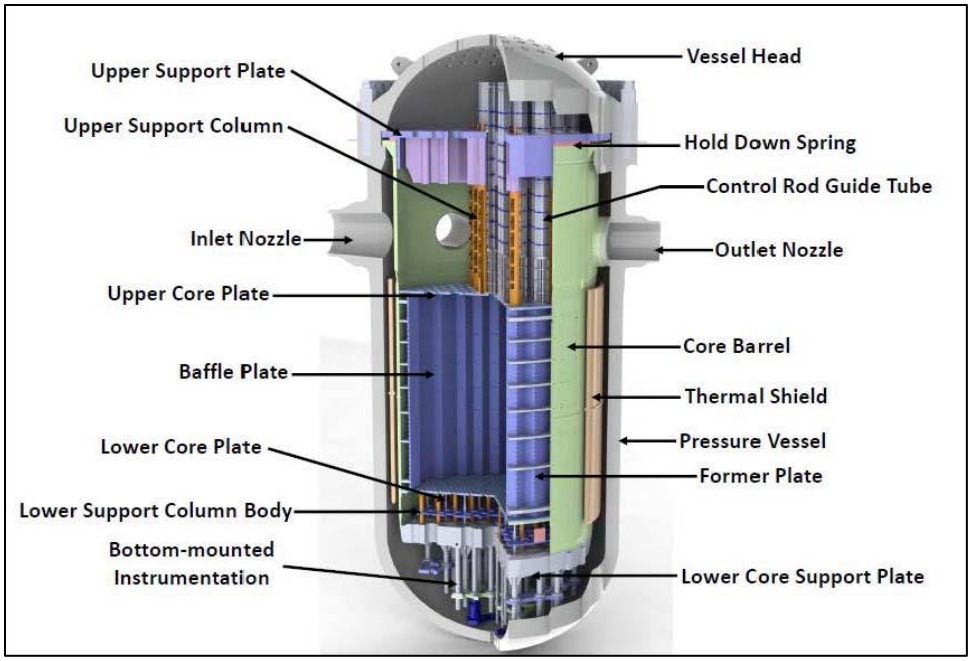

Figure 1 - Illustration of Typical Pressurized Water Reactor Assembly

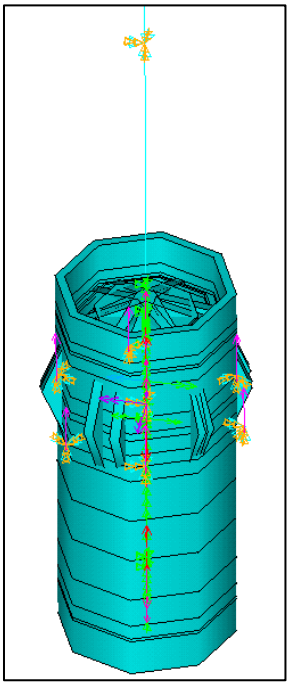

Figure 2 - Illustration of System Finite Element Model

For purposes of the sensitivity analysis, the model was parameterized as follows. The input parameters of interest correspond to model features such as stiffness, damping, gap dimensions, and masses, which vary between various otherwise-similar PWR Reactor Vessel Internals (RVI) structures. In some cases, this variation represents a true change in the underlying physical parameter, thus constituting an aleatory uncertainty. In other cases, the variation represents the differences imposed to the finite element model in order to bound the plausible scatter, so as to achieve conservative design margins; these basically represent epistemic uncertainties. The response quantities of interest are related to lateral acceleration of the Reactor Vessel Closure Head (RVCH), which is denoted as "Vessel Head' in Figure 1 and represented by a mass element in Figure 2.

A preliminary GSA was performed with 16 potentially-important input parameters, and those 16 parameters were down-selected to the six parameters which best account for the variance in the model response of interest. The choice to use 6 rather than 16 parameter is intended to more clearly illustrate the surrogate modeling and GSA process, although it is recognized that the surrogates could have been trained and this GSA performed using all 16 parameters. The truncated set of parameters is briefly described in Table 1. Specifically, the response quantity of interest for this analysis is P17 (acceleration of RVCH) and so $k(\theta)_3$, ζ, $g(y)_5$, k_9, and k_{10} constitute the input parameters most strongly correlated with P17. For the GSA simulations performed with this SFEM, the parameters were varied ±5% about their nominal value (sampled from a Uniform distribution), to account for their typical range of variation

between many operating PWRs, and the extent to which these parameter can change during reactor aging. A Uniform distribution was employed to represent the assumption that the magnitude any of the selected parameters is expected to have an equal probability of falling anywhere within the range of ±5% about its nominal value.

Table 1 - SFEM Parameters

Parameter Number (per finite element modeling)	**Description** [(1)]	**Identifier**
P4	Rotational Stiffness for Core Support (Denoted Location 3)	$k(\theta)_3$
P10	Damping	ζ
P11	Vertical Gap at Support Flange (Denoted Location 5)	$g(y)_5$
P12	Number of Features in Upper Plenum (Denoted Location 6)	N_6
P15	Stiffness at Pressure Vessel (Denoted Location 9)	k_9
P16	Stiffness at Piping (Denoted Location 10)	k_{10}

Note:

1. The location identifiers are left intentionally generic in this dissertation so as to protect information which may be considered proprietary. It is judged adequate for purposes of this research to merely identify locations with generic numbers.

The loading considered on the system corresponds to a LOCA, which is a non-stationary event in which the mean value and frequency content of the excitation is time varying. The U.S. N.R.C. defines a LOCA as "Those postulated accidents that result in a loss of reactor coolant at a rate in excess of the capability of the reactor makeup system from breaks in the reactor coolant pressure boundary, up to and including a break equivalent in size to the double-ended rupture of the largest pipe of the reactor coolant system." Sample load histories and their corresponding power spectra for two different power generation units are shown near the reactor vessel inlet and within the

core support structure region in Figure 3 and Figure 4, respectively, as determined from an un-steady thermal-hydraulic analysis performed using MULTIFLEX (24). It should be noted that, because these histories are non-stationary, the power spectra in Figure 3 and Figure 4 do not fully describe the process. Given these non-stationary excitations, the transient response of the RVCH was evaluated through the SFEM with typical response histories shown in Figure 5 for different values of the input parameters.

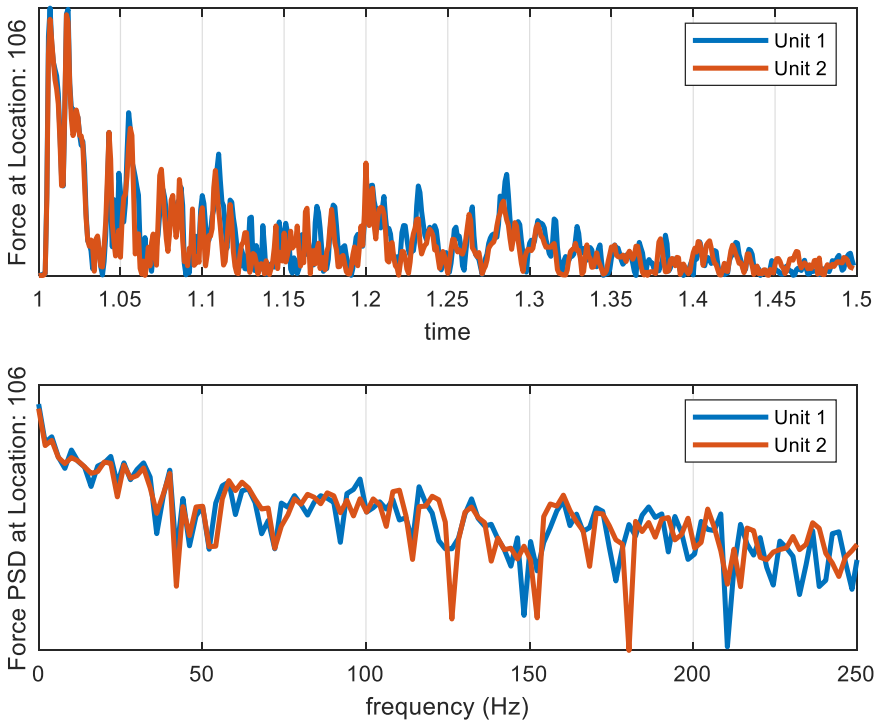

Figure 3 – Typical LOCA Forcing Function near Reactor Vessel Entrance

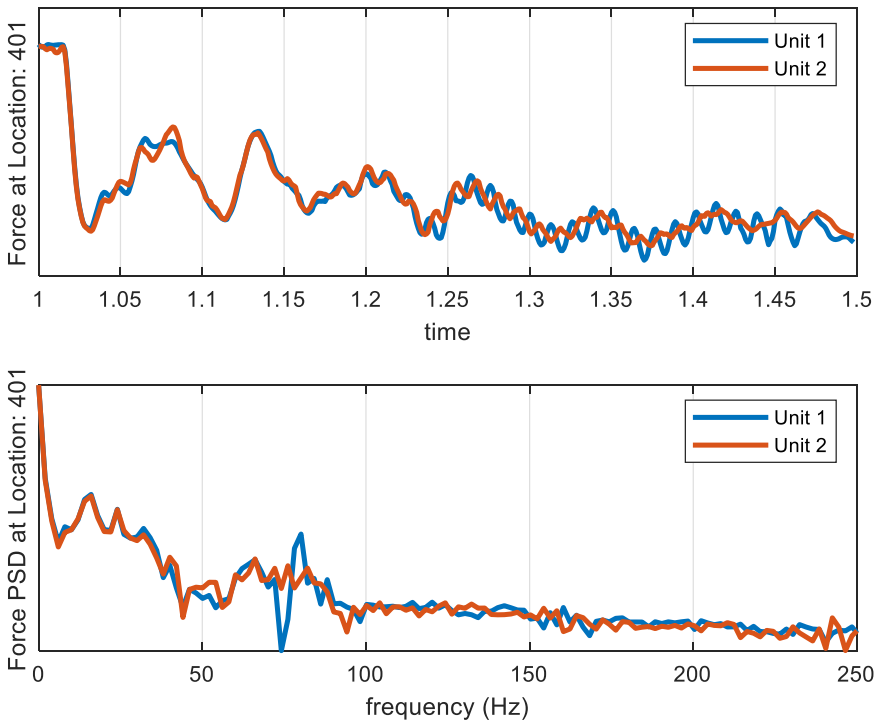

Figure 4 - Typical LOCA Forcing Function within Core Support Structures

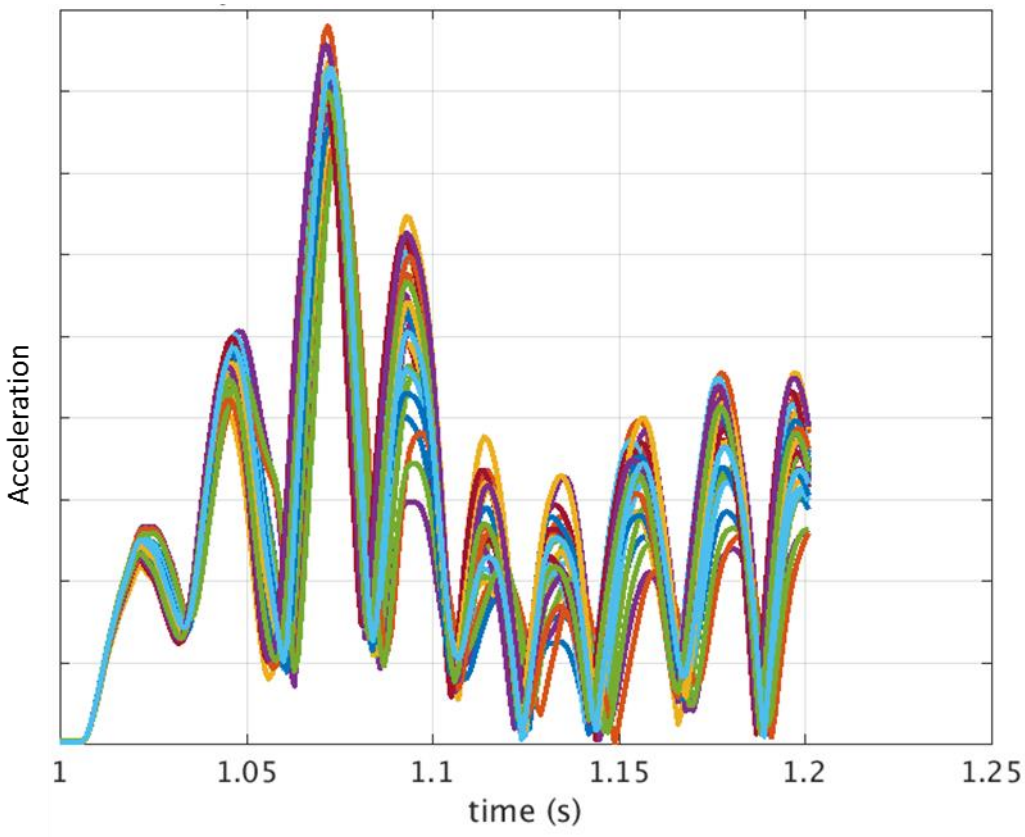

Figure 5 - Acceleration Time Histories for RVCH lateral motion, where each line shows a different sample of the random parameters. Note that units are not provided due to information release restrictions.

Two important metrics of response are extracted from the RVCH lateral acceleration time histories. The first is the peak acceleration. The second is the peak first-mode amplitude of the acceleration response spectrum. The response spectrum method is important for understanding the response of components attached to the RVCH, but not explicitly modeled in the SFEM. It is the primary approach used for characterizing the response of such components in the nuclear industry, such as described in Paragraph N-1110(d) of (1).

In practice, response spectra are used in dynamic analyses of nuclear power plants (25), and can be computed using such software as (26). Upon completion of the

transient (i.e., time-domain) finite element analysis, the lateral acceleration response of the RVCH is used as base excitation for a single degree-of-freedom (SDOF) system having natural frequency ω_0 and the absolute maximum acceleration of the SDOF system is retained. This calculation is repeated for a range of natural frequencies, and the absolute maximum acceleration at each frequency is plotted as a function of frequency. The resultant plot is the acceleration response spectrum. Sample acceleration response spectra for different values of the input parameters are shown in Figure 6. Here, we are specifically interested in the peak first-mode response of the acceleration response spectrum. That is, we study the sensitivity of the magnitude of the first peak (corresponding to the lowest frequency) in Figure 6 to the six input parameters presented above.

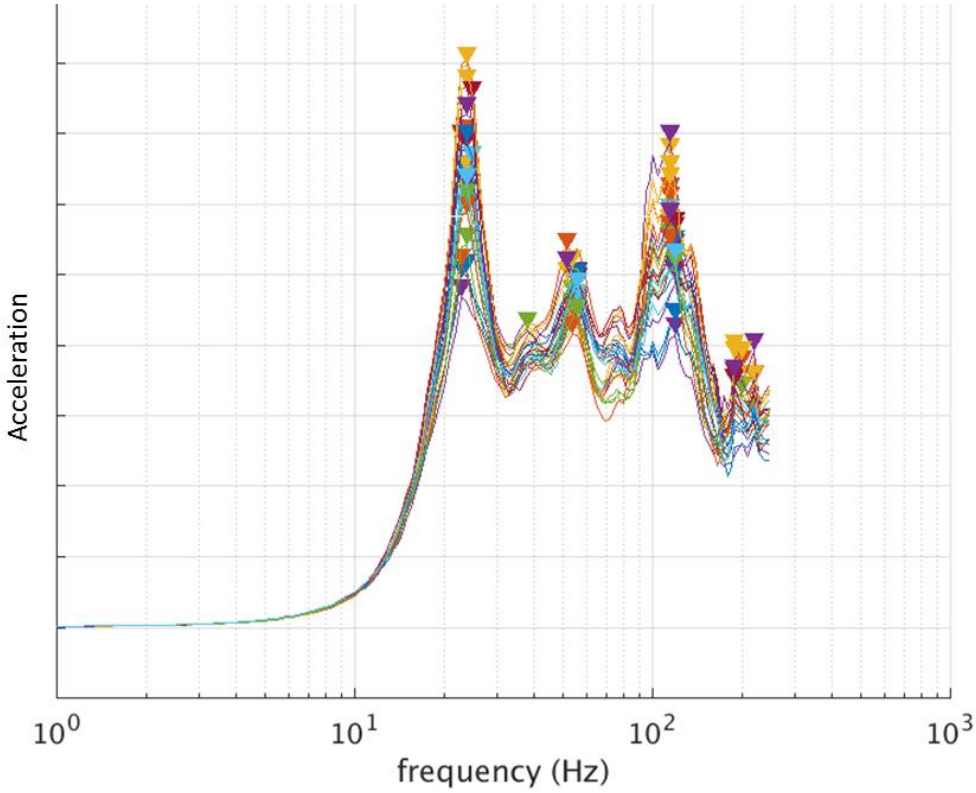

Figure 6 - Acceleration Response Spectra Overlay of RVCH Lateral Motion, where each line shows a different sample of the random parameters. Note that units are not provided due to information release restrictions.

GLOBAL SENSITIVITY ANALYSIS WITH THE FOURIER AMPLITUDE SENSITIVITY TEST

While many methods of sensitivity analysis exist (27), GSA is employed herein as a variance-based technique, which surveys the full parameter space by evaluating all values each parameter could have with respect to one another, considering the probability distribution defined for each parameter. For this application, GSA provides insight as to the relative importance of multiple parameters (e.g., stiffness, gap

dimension, damping), which mutually influence the forced response of interest. Furthermore, GSA accounts for uncertainty in the input parameter space so that each plausible combination of relative parameter variations is considered.

First-order sensitivity indices for output $y = f(\boldsymbol{P})$ given input parameters $\boldsymbol{P} = (p_1, p_2, \dots, p_n)$ are defined as (4):

$$S_i = \frac{V[E(y|p_i)]}{V(y)} \tag{1}$$

where $V[]$ denotes the variance operator and E denotes the expected value. The variance of y may be taken from the span of results across the parameter space. The expected value of y can be evaluated by the n dimensional integral:

$$E(y) = \int_{I^n} f(\boldsymbol{P}) d\boldsymbol{P} \tag{2}$$

in which I^n is the n dimensional unit hypercube. The Fourier amplitude sensitivity test (FAST) method is one of the methods used for the present study to approximate Equation (2).

The essence of FAST is to generate a curve in the parameter space that is a periodic function of each parameter, with a different frequency for each. The contribution of each input is measured by the contribution of its characteristic frequency Ω_i to the outputs per (28) and (27), and implemented into software tools such as (7). FAST involves the computation of Fourier coefficients which can be estimated by numerical integration of:

$$C_{k_i} = \frac{1}{2\pi} \int_{-\pi}^{\pi} f(s) e^{-j2\pi k_i \Omega_i s} ds \tag{3}$$

The number of discrete intervals used to evaluate this integral is defined by variable M, corresponding to the number of model evaluations, which is used as $s = {}^{2\pi q}/_{M}, \quad q = 1,2, \dots, M$. Per (29), the choice of M and the number of inputs k govern the number of model runs used to compute the global sensitivity indices. Finally, the numerator of Equation (1) needed for computing the global sensitivity indices is calculated as:

$$E(y|p_i) = \sum_i \left|C_{k_i}\right| \tag{4}$$

Substituting Equation (4) into Equation (1) provides first-order global sensitivity indices:

$$S_i = \frac{V\left[\sum_i \left|C_{k_i}\right|\right]}{V(y)} \tag{5}$$

SURROGATE MODELING WITH GAUSSIAN PROCESS REGRESSION

This study also utilized Kriging, otherwise known as Gaussian process modeling or Gaussian process regression, for the surrogate modelling component, as it has been shown to be effective for stochastic structural dynamics (30). In particular, Kriging has the advantage of providing an error metric in the variance of the surrogate model, and has also been successfully integrated into methods of sensitivity analysis (5).

A Kriging model, $\mathcal{M}^K$, serving as a surrogate for the full-order model $\mathcal{M}$ (e.g., the peak acceleration from the random vibration finite element model, $\ddot{u}_p$), is expressed as outlined in (31), (32), and (33), by:

$$\mathcal{M}^K(x) = \boldsymbol{\Psi}(\boldsymbol{x}) + \sigma^2 \boldsymbol{Z}(\boldsymbol{x}, \xi) \tag{6}$$

in which bold-faced variables indicate vector quantities, $\boldsymbol{\Psi}(\boldsymbol{x})$ is the mean value (or trend) constructed from regression coefficients $\boldsymbol{\beta}$ and basis functions $\boldsymbol{f}(\boldsymbol{x})$, which is computed as the summation:

$$\boldsymbol{\Psi}(\boldsymbol{x}) = \sum_{\alpha \in \boldsymbol{A}^{M,P}} \beta_\alpha f_\alpha(\boldsymbol{x}) \tag{7}$$

where the basis functions were taken as multivariate polynomials of the form $f_\alpha(\boldsymbol{x}) = \prod_{i=1}^{M} {x_i}^{\alpha_i}$, $\boldsymbol{\alpha} = \{\alpha_1, \alpha_2, \dots, \alpha_M\}$ is a vector of indices, and $\boldsymbol{A}^{M,P} = \{\boldsymbol{\alpha}\colon |\boldsymbol{\alpha}|_1 \leq P\}$ that yield polynomials in the M input variables up to degree P.

The second term in Eq. (6), $Z(\boldsymbol{x}, \theta)$ is a zero-mean stationary Gaussian random process with variance σ^2 and autocorrelation function $R(\boldsymbol{x}; \boldsymbol{\theta})$ with which a correlation matrix $\boldsymbol{R}$ is populated.

Maximum Likelihood Estimation (MLE) is used with a specified trend and correlation function, and a Kriging surrogate is established by estimating parameters β (for trend), and σ^2, θ (for correlation) which maximize the likelihood of realizing the actual (known) function evaluations (i.e., from full-order model $\mathcal{M}$). The operations by which MLE is used to perform this calculation are detailed in (33) or (34).

DESIGN OF EXPERIMENT SAMPLING

A critical component to creating any surrogate model, including Gaussian Process Regression, is the training dataset. The surrogate model is only as good as the training dataset, and therefore, the dataset should be ensured to contain the important

features of the system of interest. However, it is also important to attempt to minimize the size of the training dataset required, as generating this data is typically the most computationally demanding aspect of the problem. Different variants of stratified sampling are studied herein. In stratified sampling, the sample space for an input parameter is divided into strata, and input values are obtained by sampling separately from within each stratum instead of from the distribution as a whole, as is done for random Monte Carlo sampling. It has been shown that stratified sampling methods, such as LHS, can yield substantially improved sampling errors in terms of properly characterizing a probability density function with a given number of samples (35). In fact, for univariate analysis it has been shown that the sampling error of Monte Carlo goes down as the order of $\frac{1}{\sqrt{N}}$, whereas the sampling error for LHS decreases as the order of $\frac{1}{N}$ per (36) and (37), for example.

Specifically, the training data sets were generated by exercising a full-order SFEM for which computational DOEs were constructed using Latin Hypercube Sampling (LHS) and a generalized Latin Hypercube sampling method called Latinized Partially Stratified Sampling (LPSS) (38).

Latin Hypercube Sampling

In contrast to random Monte Carlo sampling, LHS aims to spread the sample points evenly across all possible values (39). One of its first implementations was in a Sandia National Laboratory computer program simply titled “Latin Hypercube Sampling”

(35). As a version of stratified sampling, LHS partitions each input parameter distribution into intervals of equal probability, and selects one sample from each interval, and shuffles the sample for each input so that there is no correlation.

Latinized Partially Stratified Sampling

The LPSS method developed in (38) performs simultaneous Latin hypercube sampling of all variables and stratified sampling of subsets of variables, and has been shown to provide variance reduction in the context of parameter interactions (38).

LPSS is achieved by first defining a partially stratified sampling (PSS) design, as described in Section 3 of (38), and as follows. Let $\Theta_i, i = 1, \dots, N_S$ denote N_S disjoint N_i-dimensional orthogonal subspaces of the N-dimensional sample space. PSS divides each subspace Θ_i into a collection of M_i disjoint subsets $\Xi_{ik}; k = 1,2, \dots, M_i$. Lower N_i dimensional random samples $\boldsymbol{p}_{ik} = \{p_{ik1}, p_{ik2}, \dots, p_{ikN_i}\}$ are generated within each stratum Ξ_{ik} of subspace Θ_i according to the stratified sampling method. Then, full N-dimensional samples $\boldsymbol{p}$ are assembled by randomly grouping the lower-dimensional samples generated in each subspace. The most significant challenge to PSS is to identify the optimal subspace decomposition. In some cases, it may be clear which variables are interacting which will inform the PSS subspace definitions, but such cases are the exception. Indeed, the variables which are interacting are not known *a priori* in the present work applied to nuclear reactor internals structural dynamics. Coupling PSS with "Latinized" stratified sampling (LSS) helps to alleviate this concern.

LSS permits one to simultaneously reduce variance associated with both the main and interaction effects by constructing, on a given N_i-dimensional subspace, a true stratified sampling design that is at the same time an LHS design. The procedure for accomplishing this is described in Table 2.

Table 2 - LSS Method Procedure

Step	Description
1	Draw an LHS from the subspace
2	Stratify the domain as desired ensuring that the stratification is consistent with an LHS design
3	For each stratum, randomly select a point p_i from each component of the LHS (without replacement) such that the sample $p = \{p_1, p_2, \dots, p_N\}$ lies within the stratum
4	Repeat for each stratum of the design.

Finally, LPSS involves the use of LSS in combination with PSS. Following the definition of a PSS design, samples from the lower-dimensional subspaces are then drawn according to the LSS method. Thus, with LPSS, it is sufficient to stratify a set of variables together simply based on the possibility that they may interact. If the chosen parameters do interact then the savings, in terms of variance reduction (and associated accuracy of surrogate model and GSA, in this application), will be amplified by reduction in both the main effects and interactions. If the chosen parameters do not interact, there will be no increase in variance since the main effects are also being filtered thanks to LSS.

SFEM-based PWR Global Sensitivity Analysis

Given the six parameters which most influence the model result of interest, a fractional-factorial DOE (40) was constructed in order to quickly identify which parameters possess interactions to thus inform the subdomain arrangement for LPSS. Given those observations, the subdomains for LPSS were set up as shown in Table 3.

Table 3 – Subdomain Composition for LPSS of SFEM

Model parameters	**sub-domain dimension** (N_i)
P4 $k(\theta)_3$ P15 k_9 P16 k_{10}	3
P10 ζ P11 $g(y)_5$ P12 N_6	3

From the subdomains defined in Table 3, the number of strata Ξ_{ik} were set to 3, 4, 5, 8, 10, and 12. Therefore, the resultant number of samples was $N_i^{\Xi_{ik}} = 27$, 64, 125, 512, 1,000, and 1,728, respectively.

Sensitivity Analysis

Having demonstrated in (15) the successful use of a Surrogate model to perform GSA for a reactor upper internals (UI) flow-induced vibration (FIV) model, a similar approach is employed for the SFEM, as illustrated in Figure 7. This approach is similar in principle to that applied to the stationary UI FIV finite element analysis in the sense that Kriging surrogates were developed through LHS and LPSS. Hence, the objective of this study is to rigorously compare GSA performed using sparsely sampling (LHS and LPSS) based surrogate models with more direct full-order model driven FAST GSA.

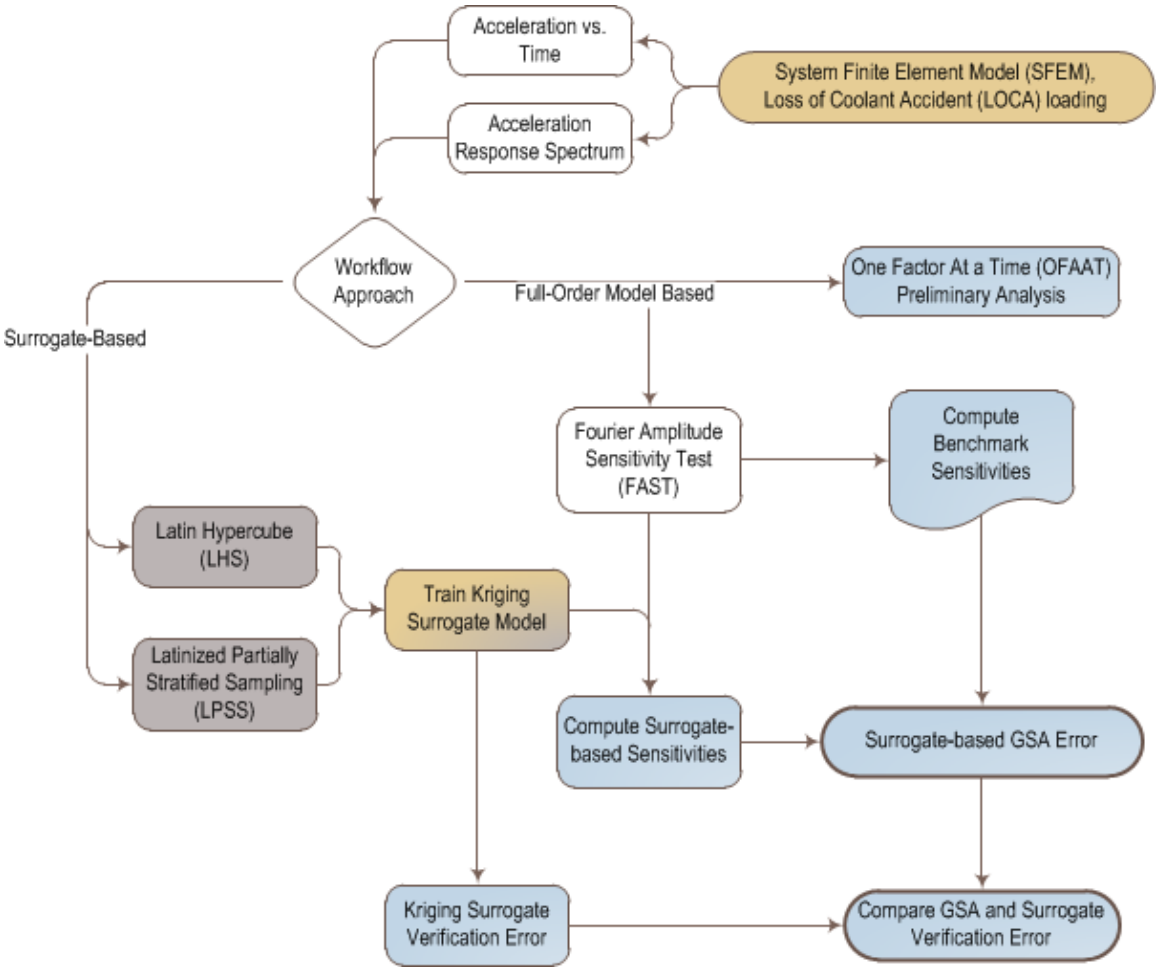

Figure 7 - Flow Diagram of Surrogate Modeling, Sensitivity Analysis, and Error Evaluations

As previously noted, GSA requires that a model be executed numerous times through a computational DOE to permit direct computation via FAST, or the training of surrogate models for use in GSA calculations. As such, it could be argued that the insight provided by GSA is somewhat diluted by the computational expense of performing GSA, relative to simply varying one factor at a time. Therefore, in the interest of motivating the use of GSA for this application, of preliminary interest is quantification of the percent change in model outputs when a single input parameter is varied as a one factor at a time (OFAAT) sensitivity analysis. Figure 8 shows how the lateral RVCH motion changes, relative to the nominal values of three stiffness

parameters listed in Table 1. It may be seen that the structural dynamic system behavior is indeed non-linear with respect to the ±10% range of variation on the three selected input parameters, $k(\theta)_3$, k_9, and k_{10}. Examination of Figure 8 could lead one to conclude input parameter $k(\theta)_3$ to be of far higher relative importance to k_9 and k_{10}. While such a conclusion would be true if varying one factor at a time, that inference may not necessarily be true for cases in which multiple factors possess uncertainty, and thus could vary from their nominal value. That is, interaction and combinatorial effects could produce significant non-linearities in model output trends which would motivate one to consider GSA which surveys the full parameter space considering all possible combinations of input parameters. Such a GSA is presented in the following sections.

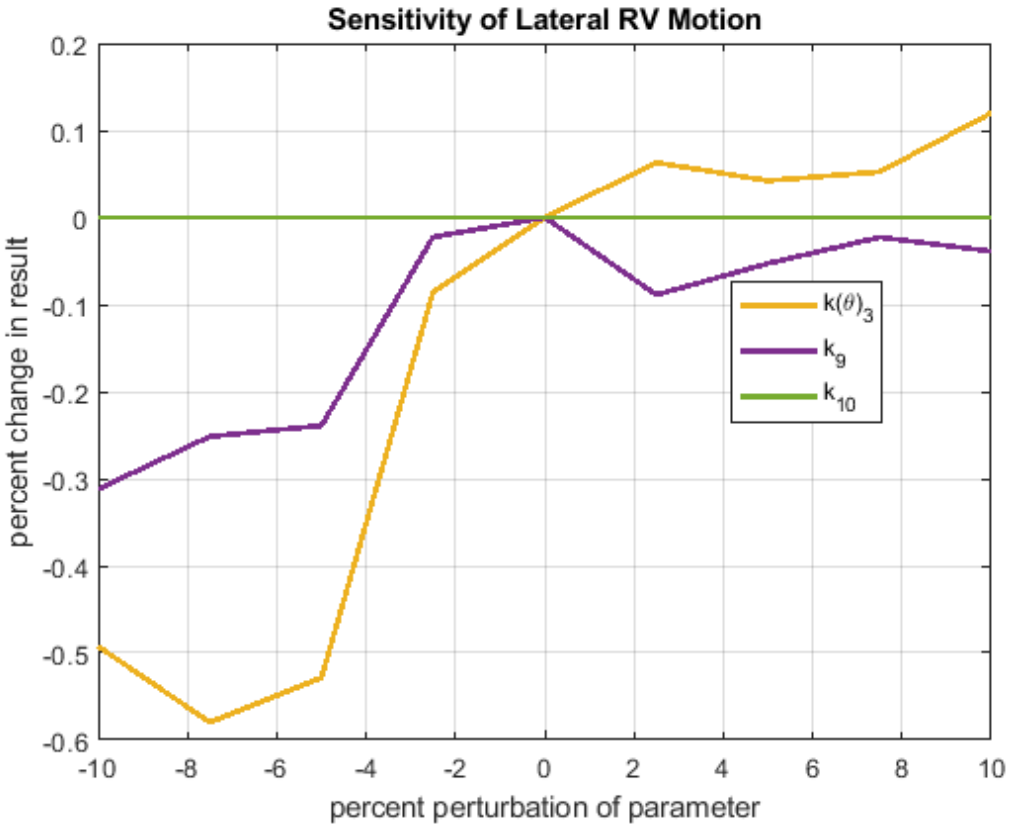

Figure 8 - Single Factor Sensitivity of Lateral RV Motion with respect to Three Stiffness Parameters Varied by ±10%

SENSITIVITY ANALYSIS OF FULL-ORDER MODEL USING FAST

Prior to evaluating the effectiveness of model training approaches on GSA results computed from a surrogate model, we establish a benchmark set of GSA results using the FAST algorithm directly applied to the SFEM. Figure 9 shows the full-order SFEM GSA first-order sensitivities using FAST with 5,000 and 8,000 samples from which it can be seen that the difference in sensitivities upon changing sample size is negligible, indicating convergence of the sensitivity indices. Unlike the GSA results presented in (15) in which three of the six parameters imparted nearly zero variance to the model

output of interest, five of the six parameters included in the SFEM GSA contribute at least 5% variance to the model output of interest (P17, peak lateral acceleration of the RVCH). Referring to Table 1 for the parameter identifiers, it may be seen that stiffness between two components in the reactor system k_9 (P15) carries the greatest sensitivity, following by the number of components, N_6 (P12). Terms k_9 and N_6 are local features of the system associated with specific components, but they impart a significant influence on results of interest. Meanwhile, damping (ζ) which is a system level parameter, shows a non-negligible sensitivity, but is appreciably smaller than the local features k_9 and N_6. This insight on the relative sensitivity of damping is somewhat unexpected in the sense that damping is often perceived to impart greater variations than such local quantities, which was not the case here.

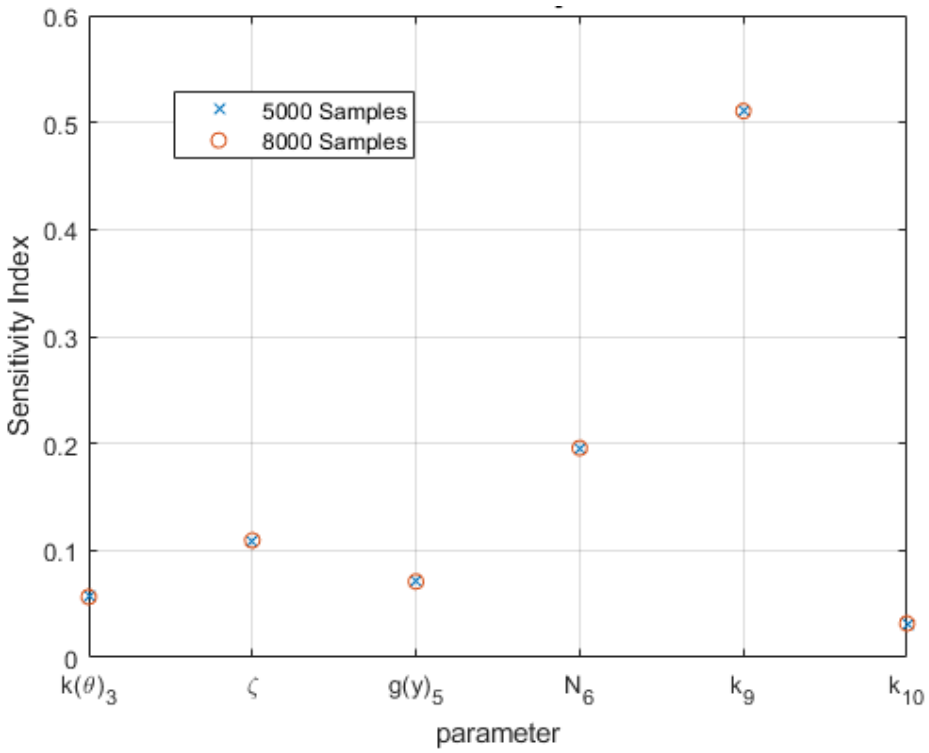

Figure 9 Full-Order Model GSA Results for SFEM using FAST

SURROGATE-BASED SENSITIVITY ANALYSIS

Having thus established stable GSA results for comparison to those computed from surrogate models, Figure 10 shows the Kriging-based GSA results with bars and the associated full-order model based FAST GSA results shown with black circles. The figure shows results using both LHS and LPSS for increasing sample sizes, from which it may be seen that, even for small sample sizes (as low as 27 samples), the sensitivity indices are approximately correct and very accurate sensitivity indices can be obtained with very small sample sets (64 or 125 samples). Note that sample sizes were determined by the stratification of the domains for LPSS, as shown in Table 3.

In order to better visualize the surrogate-based GSA error indicated in Figure 10, Figure 11 and Figure 12 show the difference between the surrogate-based GSA results and those from the full-order model as a bar graph and line plot, respectively. While the accuracy associated with LHS and LPSS is nearly equivalent at sample sizes of 125 or greater, the LPSS results appear to show generally lower error for sample sizes of 27 and 64 – although the difference is not particularly large.

The shape of this response surface may serve to clearly illustrate the value of GSA as opposed to single-factor sensitivities (i.e., the line plots shown in Figure 8), as the two terms have a compounding and non-linear effect with respect to one another. That is, k_9 (P15) and N_6 (P12) have a combined effect on the RVCH acceleration (P17) which is complex, and which could easily be misunderstood if all factors were held constant except for one. This effect is further illustrated by considering the combined

influences that k_9 and k_{10} have on the same result, as shown in Figure 13, where the effect that P16 imparts on output P17 depends on the value of P15.

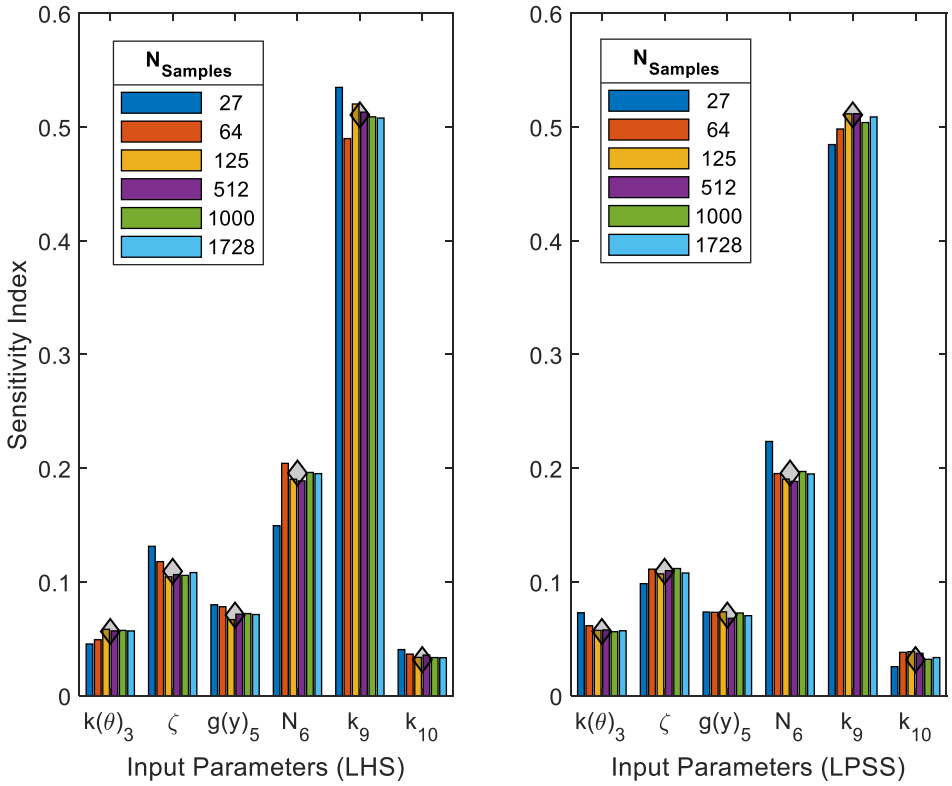

Figure 10 - Surrogate-based GSA Results for SFEM Maximum Acceleration, Compared to Full-Order GSA Results (indicated using diamond symbols), using LHS (Left) and LPSS (Right)

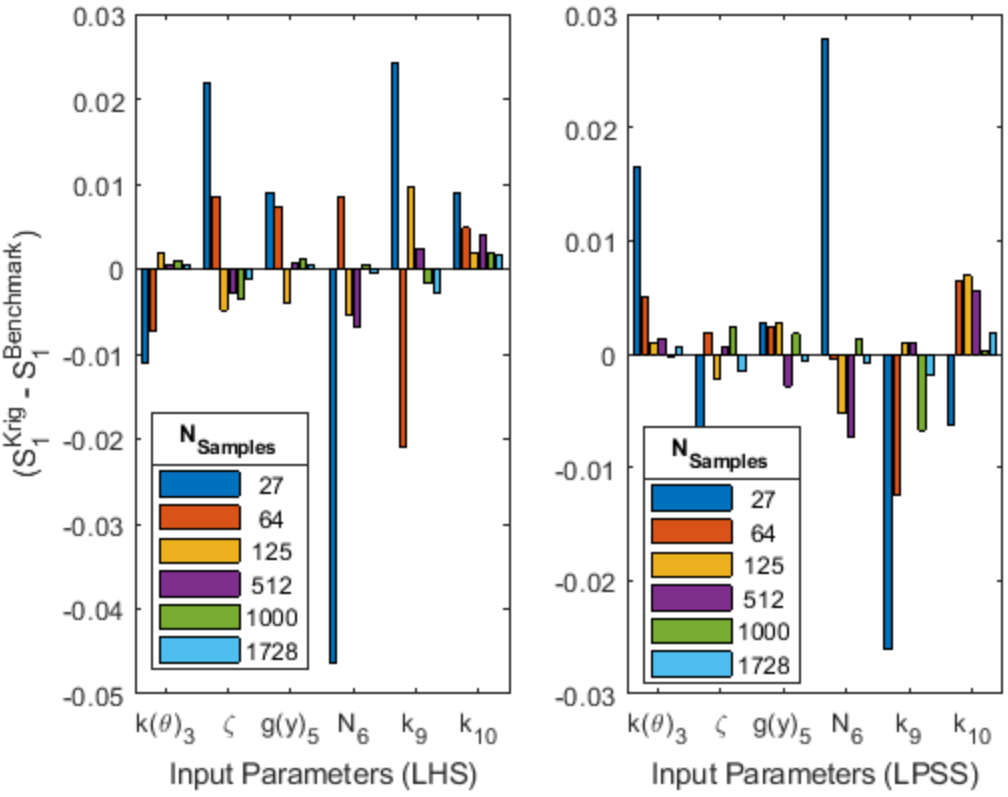

Figure 11 - Difference between Kriging-based and Full-Order GSA Results of SFEM Maximum Acceleration (Bar Graph) using LHS (Left) and LPSS (Right)

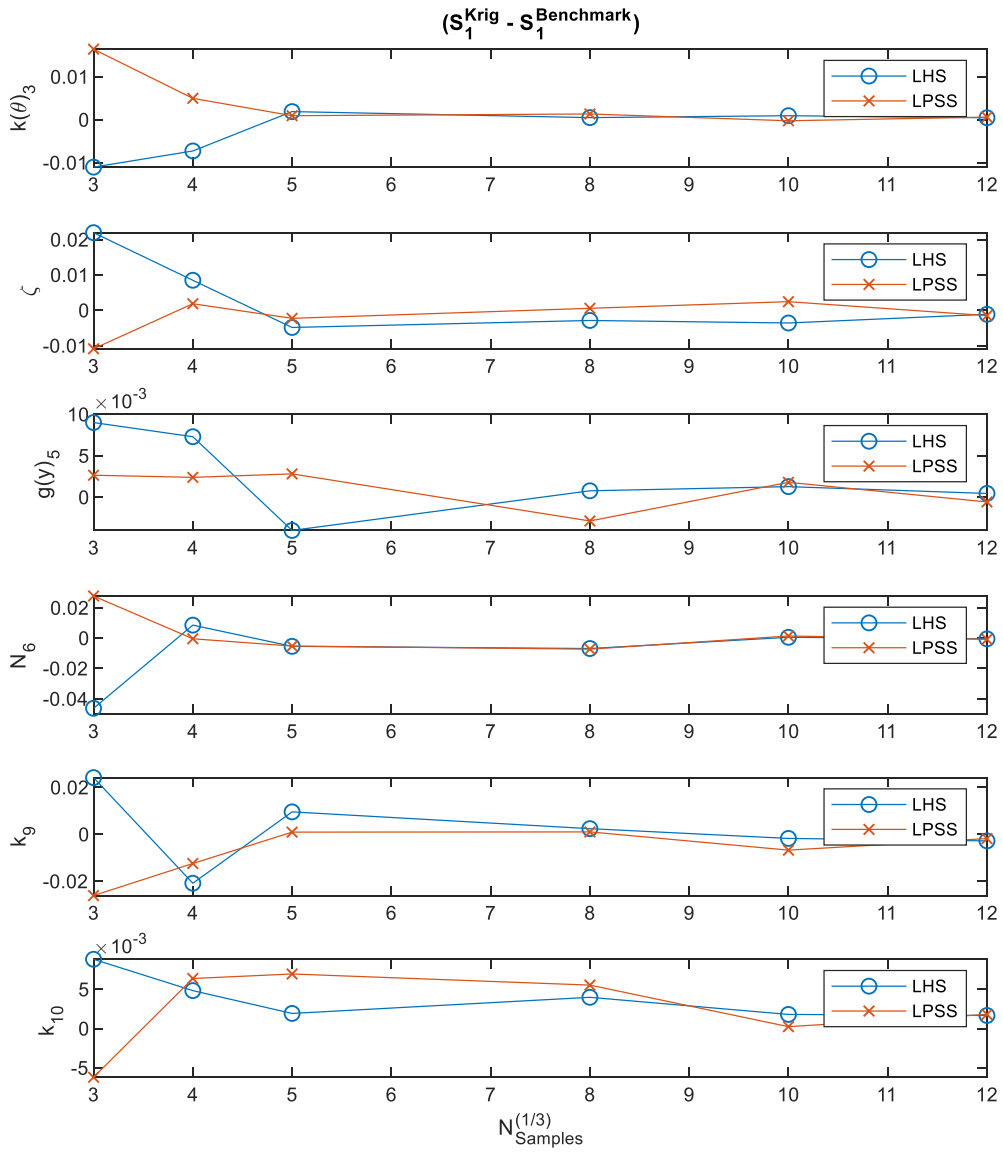

Figure 12 - Difference between Kriging-based and Full-Order GSA Results of SFEM (Line Graph)

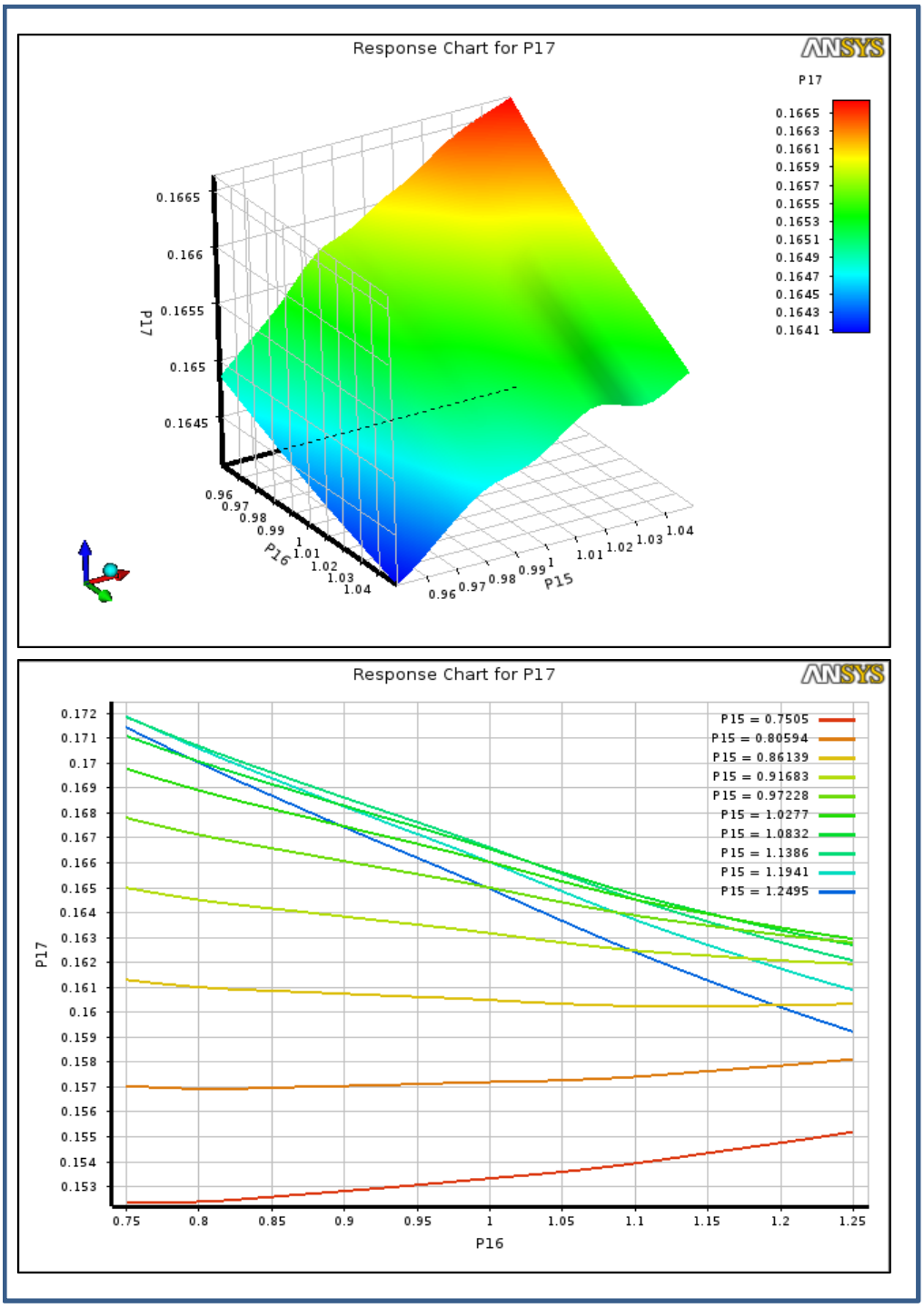

Figure 13 - Illustration of Kriging Surface Variation for RVCH Lateral Acceleration (P17) with respect to k_{10} (P16) and k_9 (P15)

SURROGATE MODEL ACCURACY

Having thus established that both LHS and LPSS provides sampling strategies from which accurate GSA results may be computed from a surrogate model, it is of interest to quantify the verification error associated with the surrogate model itself. Provided m values of the finite element model result y and surrogate model result $\hat{y}$, define Relative Root Mean Squared (RMS) error as $\sqrt{\frac{1}{N}\sum_{i=1}^{m}\left(\frac{y_i-\hat{y}_i}{y_i}\right)^2}$, and Maximum Relative Residual error as $\max_{i=1:m}\left(\left|\frac{y_i-\hat{y}_i}{y_i}\right|\right)$. Using the Relative RMS and Maximum Relative Residual error metrics for the SFEM surrogate models, Figure 14 illustrates how the surrogate model accuracy generally improves with an increasing number of samples, considering a relatively small ±5% range of variation on the input parameters. Consistent with prior observations, the surrogate model verification error associated with LPSS is lower than that for LHS at the lower sample sizes of 27 and 64.

Figure 15 then shows a plot of surrogate model accuracy, but with a larger ±25% range of variation on the same input parameters. The improvement in surrogate model accuracy with LPSS compared to LHS is even more significant than for the larger range of parameter variation. For example, at 27 samples the surrogate verification error is approximately 50% lower for LPSS than for LHS with ±25% parameter variation, whereas the surrogate verification error is approximately 20% lower for LPSS than for LHS with ±5% parameter variation. The difference between the ±5% and ±25% case is consistent with the interaction effects also being more significant with a larger range of variation. Such consistency is considered reasonable as the stronger interaction effects manifest

themselves in effective variance reduction provided by LPSS, and therefore a greater degree to which surrogate model accuracy is improved for smaller sample sizes, when compared with LHS.

Even at the lowest sample size of 27, the surrogate model verification error for LPSS was less than 1.5% and 3% for the Relative RMS and Maximum Relative Residual error metrics, respectively. For most practical purposes, these errors are small enough to render such a surrogate acceptable, which suggests that a mere 27 sample computational DOE can prove quite useful for this application.

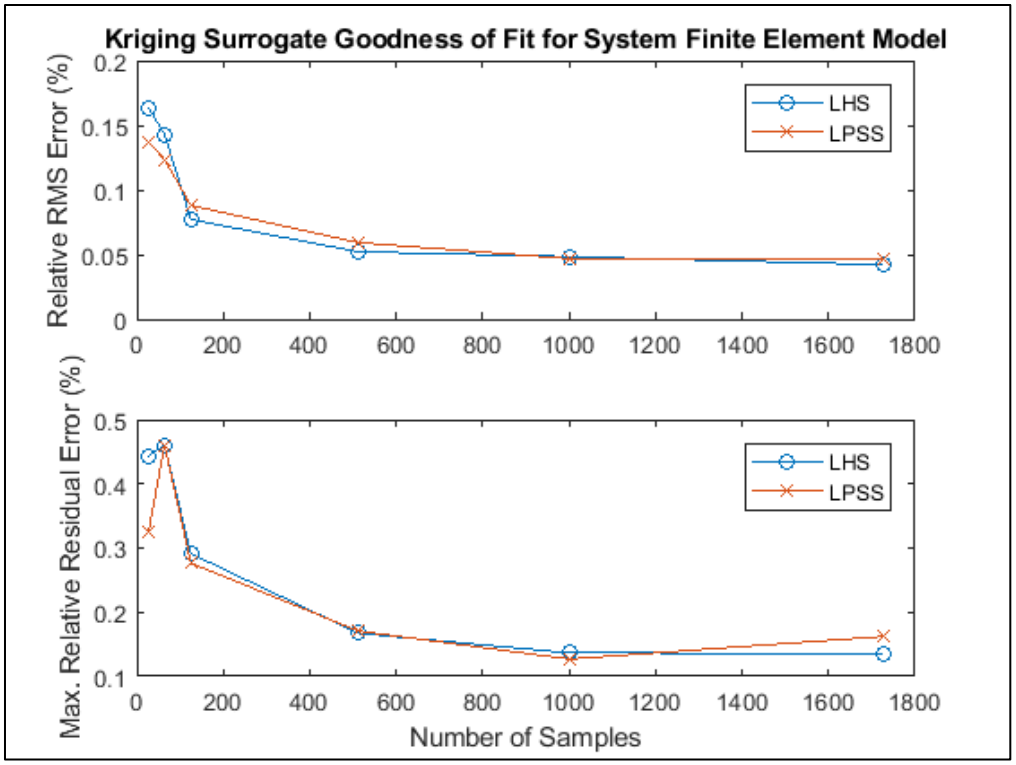

Figure 14 - Verification of Kriging Surrogate for SFEM with ±5% Input Parameter Variation

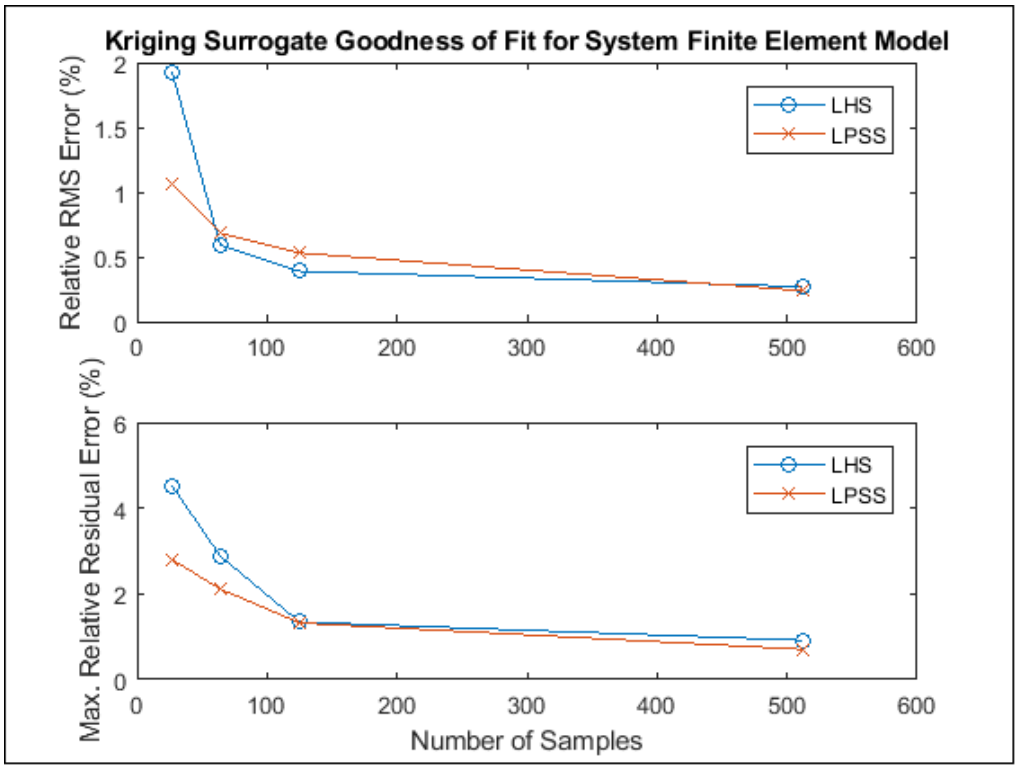

Figure 15 - Verification of Kriging Surrogate for SFEM with ±25% Input Parameter Variation

The decrease in both surrogate verification and GSA error with respect to increased sample size may be visualized in Figure 16 within which the RRMS surrogate verification error, as a percentage, is compared with the absolute value of GSA error. Thus, per Figure 16, the rate of improvement of both error metrics with respect to increasing the number of samples is comparable.

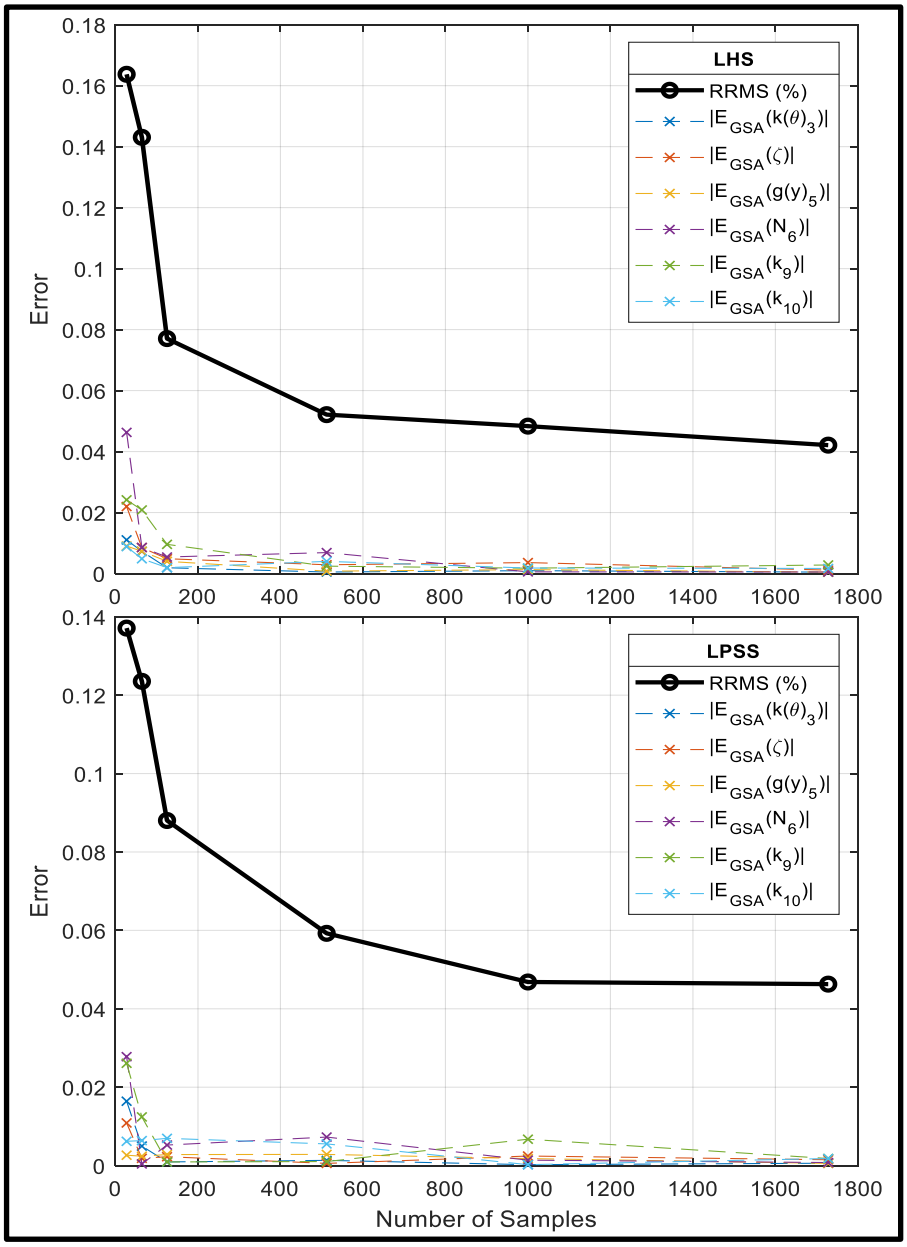

Figure 16 - Overlay Comparison of Surrogate Verification RRMS Error and GSA Error for LHS (top) and LPSS (bottom)

COMPARISON STUDY TO EVALUATE ACCELERATION RESPONSE SPECTRA SENSITIVITY

While the maximum RVCH acceleration from the transient analysis is used in practice for ASME Code design analysis of reactor equipment and is therefore the model output of interest chosen to evaluate within the preceding subsections, the magnitude of the acceleration response spectrum is also of practical engineering interest. Particularly for a SFEM which is used to develop loading for detailed sub-model stress evaluations (e.g., reactor components not explicitly resolved in the SFEM itself such as the control rod drive mechanism, and piping attached to the inlet or outlet nozzles, or components of a simplified head assembly), spectral amplitudes are important if a particular sub-model is attached the system and has a resonant frequency coincident with the amplified portion of the acceleration response spectrum. Therefore, the following explores the surrogate-based sensitivity analysis for the case in which the output of interest is the amplitude of the first vibration mode observed from the acceleration response spectrum.

Whereas the majority of the SFEM analyses presented in this work focus upon an output which is a maximum over time, this section seeks to explore the performance of these same methods but with respect to a spectral output. Figure 5 provides a typical acceleration time-history response. The acceleration value of interest from this plot is the maximum value which occurs at approximately a time of 1.07 seconds.

Maintaining parameter variations of ±5%, and focusing on the magnitude of the first resonant frequency of the acceleration response spectrum as the output of interest, Figure 17 shows the first-order FAST global sensitivities from the full-order SFEM using 8000 samples. Comparing these sensitivities to those for the maximum acceleration over time per Figure 9 reveals that the importance of parameters ζ and N_6 are significantly increased while k_9 is decreased dramatically. The remaining parameters are of near-negligible importance, and while their sensitivities were small in the maximum acceleration case, they are almost completely inconsequential for the acceleration response spectrum. The change in relative importance between the ζ, N_6, and k_9 terms likely has to do with the similarity between reactor system resonant frequencies of the associated components (i.e., the specific RVI components at location 6 or 9) and the frequency of the mode at which the maximum acceleration occurs. That is, the maximum acceleration occurs at approximately 25 Hz, and the resonant frequency of sub-components near location 6 (which pertain to N_6 in the upper region of the reactor) fall closer to 25 Hz than those at location 9 (which pertain to k_9 in the lower region of the reactor), and so variance in N_6 imparts greater variance in the acceleration response at that frequency than variance in k_9. Furthermore, the vibration amplitude is known to vary in inverse proportion to the square root of the damping ratio ζ (41), and so that parameter would likewise be expected to strongly influence the magnitude of the spectral response.

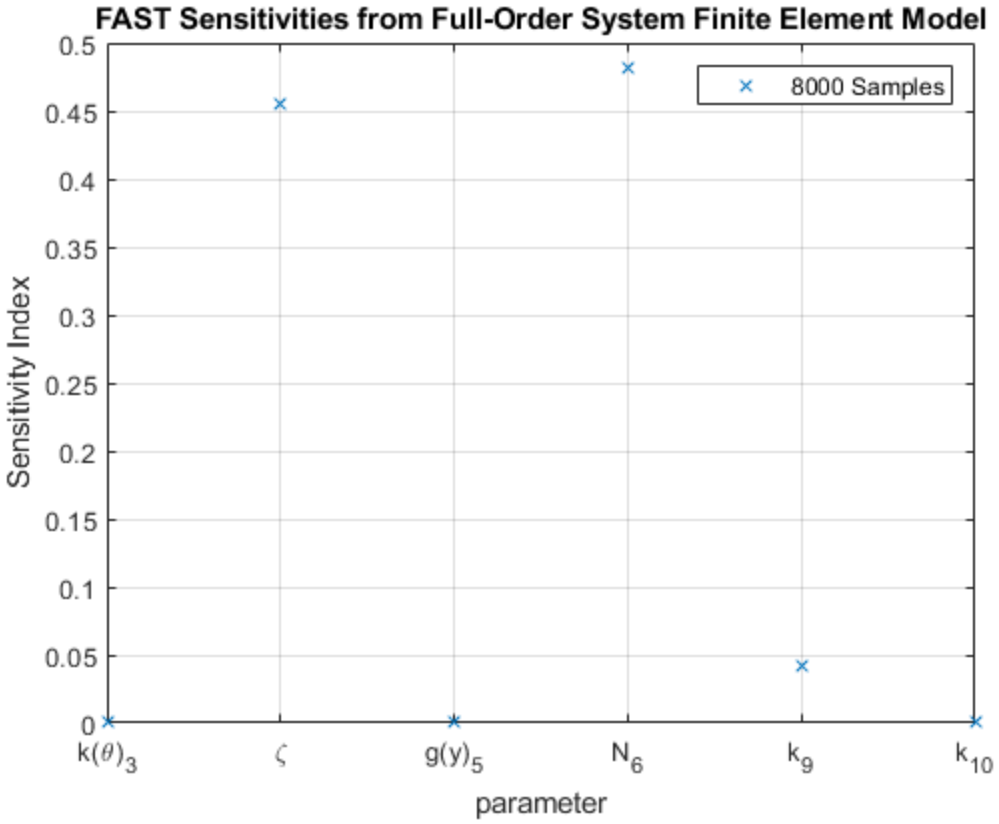

Figure 17 - Global Sensitivity Indices for System Finite Element Model Response Spectra

Similar to Figure 10 and Figure 11, but for the spectral acceleration response, Figure 18 shows the GSA results and convergence thereof for SFEM. Figure 19 shows convergence of the first-order sensitivities when Kriging surrogates are trained with LHS and LPSS for a series of training set sizes. It is apparent that at low sample sizes of 27 and 64, the GSA error associated with Kriging surrogates trained by LPSS is lower than the error for those trained by LHS. The improvement offered by LPSS makes some intuitive sense because the frequency, ω, which may be simply viewed as a function of $\sqrt{\frac{k}{m}}$ and damping, would be directly affected by combinations of parameters that affect the mass, stiffness, and damping (all six parameters studied here), and thus establishing

subdomains in which such terms are grouped according to their interactions via LPSS could result in lower errors as compared to LHS which does not establish such subdomains.

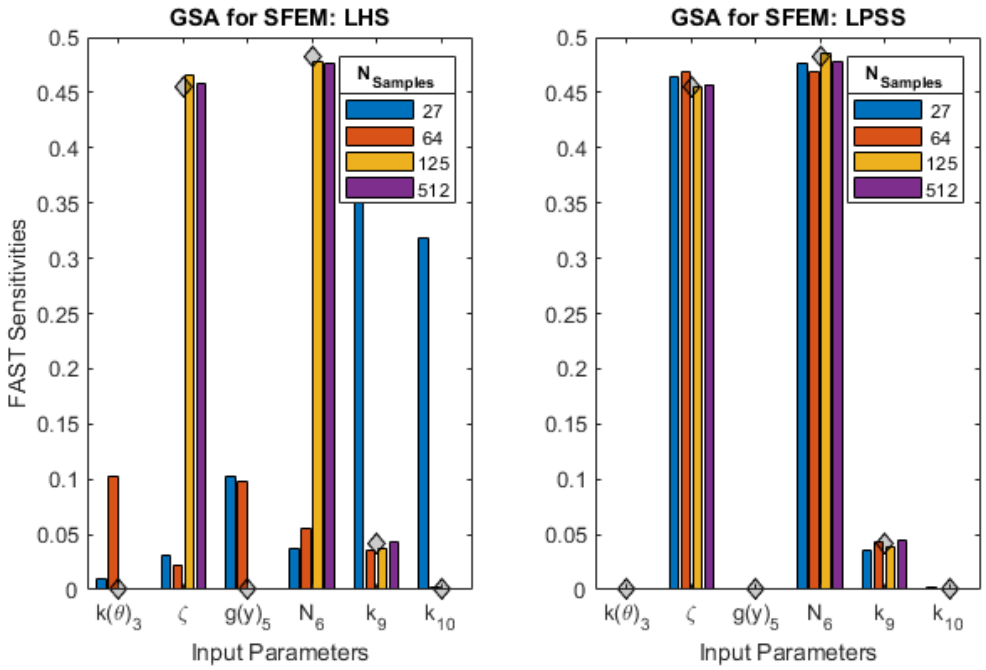

Figure 18 - Surrogate-based GSA Results for SFEM Spectral Acceleration, Compared to Full-Order GSA Results (indicated using diamond symbols), using LHS (Left) and LPSS (Right)

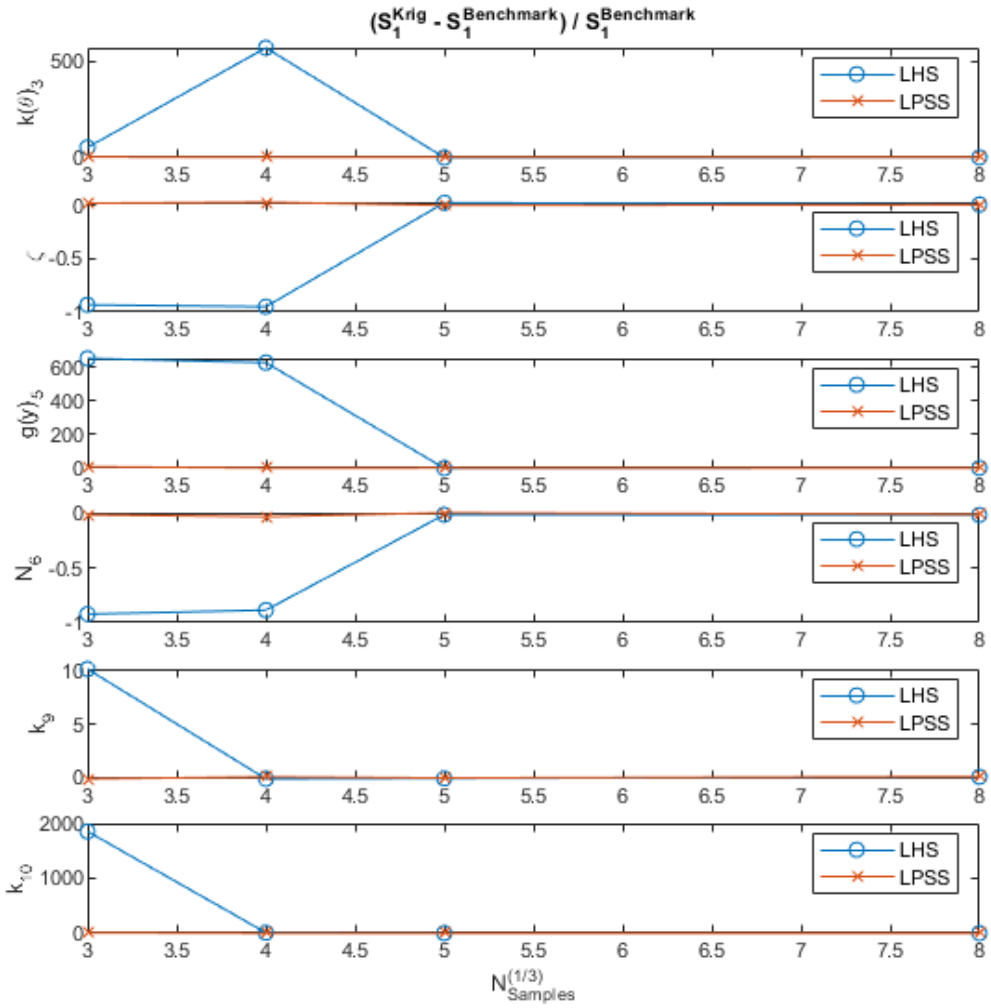

Figure 19 - Convergence of Surrogate-based Global Sensitivity Indices for System Finite Element Model Acceleration Response Spectra

Conclusion

This work demonstrates the extensibility of the surrogate-based GSA methodology shown useful for a reactor subassembly subjected to stationary random vibration in (15) to a reactor equipment SFEM, for which the finite element model included non-linearity and was subjected to non-stationary loading. The SFEM was parameterized with a total of sixteen model parameters for which there are plant-to-plant variations or for which the magnitude changes over the course of the reactor life due to aging. Of these sixteen, the six most dominant parameters were chosen to explore for the GSA studies. As a baseline case, a parameter variation range of ±5% about nominal was chosen to represent the normal amount of variation for these parameters amongst the operating fleet of PWRs, and a larger parameter variation range of ±25% was additionally studied to represent further departure from nominal values that some parameters may experience due to nuclear plant aging-related degradation mechanisms. Interaction effects were observed between those six parameters from a factorial DOE, which were used to determine the arrangement of the subdomains for LPSS.

The LPSS and LHS methods were employed to sample the parameter space from which Kriging surrogates were constructed and used to estimate GSA indices. The use of LPSS was again shown to be particularly effective at providing accurate surrogate models for very low sample sizes. For the smallest number of samples explored, and using LPSS, the magnitude of the surrogate model verification error was approximately 0.3% Maximum Relative Residual when using ±5% variation about the nominal values of model parameters (Figure 14), and less than 3% when using ±25% about nominal

(Figure 15). The corresponding Maximum Relative Residual errors associated with LHS increased to approximately 0.5% and 5%, for the ±5% and ±25% parameter variation cases, respectively. Although LHS provides a less accurate surrogate model at small sample sizes, the resultant errors may be considered acceptable for many practical engineering applications. Thus, the relatively accurate surrogate models obtained through both LHS and LPSS provides confidence in the stability of the result. Such stability in the surrogate model verification metrics suggests that the choice of sampling method is largely inconsequential if the error requirements do not demand the highest possible accuracy.

Along with the low surrogate verification errors at low sample sizes, the GSA error is correspondingly very low, measured as the difference between that computed directly from the full-order model versus that computed from surrogate models. For 27 samples, the maximum error in GSA indices was ±0.03 when evaluating the maximum acceleration of the RVCH (Figure 10), or ±0.08 when evaluating the spectral response of the RVCH (Figure 18). In either case, it is noteworthy that at such a small sample size, reasonable engineering insight can be drawn from GSA results with such small error. Similar to the surrogate model verification metrics, the GSA error likewise decreases upon increases in sample size. The agreement between surrogate model verification metrics and GSA error provides confidence that, provided a verified surrogate model, the GSA results derived from that surrogate have a low risk of inaccuracy. It is recognized that, in some situations, a benchmark model may not be practically available against which to verify surrogate model performance. This may be thought of as

somewhat analogous to situations where a computational model lacks empirical data against which it may be validated. In such situations, model credibility may be evaluated, to some extent, using methods in the field of computational modeling maturity theory described in (42), such as the predictive capability maturity method and assessment (43), (44). Nonetheless, the lack of benchmark data poses a non-negligible challenge to demonstrating credibility for computational modeling and simulation, and thus constitutes an avenue for potential future research.

REFERENCES

1. **ASME.** Rules for Construction of Nuclear Facility Components. *Boiler and Pressure Vessel Code, Section III, Appendix N.* New York, NY, USA : ASME, 2017.
2. *An Overview of PSA Importance Measures. Reliability Engineering & System Safety.* **Van der Borst, Mario and Schoonakker, H.** s.l. : Reliability Engineering and System Safety, 2001, Vol. 72, pp. 241-245.
3. *Fire probabilistic risk assessment and its applications in the nuclear power industry.* **Worrell, C. and Rochon, C.** s.l. : Fire Technology, 2016, Vol. 52, pp. 443-467.
4. **Saltelli, Andrea, et al., et al.** *Global Sensitivity Analysis: The Primer.* West Sussex, UK : John Wiley and Sons, 2008.
5. **Gratiet, L L, Marelli, Stefano and Sudret, Bruno.** Metamodel-based Sensitivity Analysis: Polynomial Chaos Expansions and Gaussian Processes. *Handbook of Uncertainty Quantification – Part III: Sensitivity Analysis, RSUQ-2016-007.* s.l. : ETH-Zurich, March 2016.
6. *Sensitivity analysis for volcanic source modeling quality assessment and model selection.* **Cannavo, F.** 2012, Computers & Geosciences, Vol. 44, pp. 52-59.
7. *A Matlab toolbox for Global Sensitivity Analysis.* **Pianosi, F, Sarrazin, F and Wagener, T.** 2015, Environmental Modeling & Software, Vol. 70.
8. **Schenk, Christian A and Schueller, Gerhart I.** *Uncertainty Assessment of Large Finite Element Systems.* Berlin : Springer-Verlag, 2005. Vol. 24.
9. *Linear random vibration by stochastic reduced-order models.* **Grigoriu, M.** 2010, International Journal for Numerical Methods in Engineering, Vol. 82.
10. *A method for analysis of linear dynamic systems driven by stationary non-Gaussian noise with applications to turbulence-induced random vibration.* **Grigoriu, M and Field, R V.** 2014, Applied Mathematical Modeling, Vol. 38.
11. **Paez, Thomas L, Tucker, S and O'Gorman, C.** *Simulation of Nonlinear Random Vibrations using Artificial Neural Networks.* Sandia National Laboratory. Albuquerque, NM : Sandia National Laboratory, 1997.
12. *Variance-based sensitivity analysis of model outputs using surrogate models.* **Shahsavani, D and Grimvall, A.** 6, June 2011, Environmental Modelling & Software, Vol. 26.
13. *Surrogate-Based Sensitivity Analysis and Uncertainty Analysis for DNAPL-Contaminated Aquifer Remediation.* **Hou, Z, Lu, W and Chen, M.** 11, November 2016, Journal of Water Resources Planning and Management, Vol. 142.
14. *Global sensitivity analysis using support vector regression.* **Cheng, K, et al., et al.** September 2017, Applied Mathematical Modeling, Vol. 49.
15. *Efficient Global Sensitivity Analysis for Flow-Induced Vibration of a Nuclear Reactor Assembly using Kriging Surrogates.* **Banyay, Gregory A, Shields, Michael D and Brigham, John C.** 2019, Nuclear Engineering and Design, Vol. 341, pp. 1-15.
16. *Development of an Advanced PWR Reactor Internals System Finite Element Model for Flow-Induced Vibration Analyses.* **Palamara, Matthew J, et al., et al.** Boston, MA : ASME, 2015. Pressure Vessels and Piping (PVP) Conference.
17. *Vibration and Stress Analysis of a UGT Assembly for the APR1400 RVI CVAP*. **Ko, Do Young and Kim, Kyu Hung.** 2012, Nuclear Engineering and Technology, Vol. 44.

18. *Structural Analysis of the CSB and LSS for APR1400 RVI CVAP.* **Ko, Do Young and Kim, Kyu Hyung.** 2013, Nuclear Engineering and Design, Vol. 261.
19. *Sensitivity Analysis of a Nuclear Reactor System Finite Element Model.* **Banyay, Gregory A, Smith, Stephen D and Young, Jason S.** Minneapolis, MN : ASME, 2018. Verification and Validation Symposium.
20. *Dynamic Pressure Inside a PWR – A Study Based on Laboratory and Field Test Data.* **Au-Yang, M K and Jordan, K B.** 1980, Nuclear Engineering and Design, Vol. 58, pp. 113-125.
21. *A Computerized Method for Flow-Induced Random Vibration Analysis of Nuclear Reactor Internals.* **Au-Yang, M K and Connelly, W H.** 1977, Nuclear Engineering and Design, Vol. 42.
22. **Au-Yang, M K.** *Flow-Induced Vibration of Power and Process Plant Components.* New York : ASME, 2001.
23. *Proposed Changes to the ASME Boiler and Pressure Vessel Code Section III Appendix N for Flow-Induced Vibrations (PVP2015-45107).* **Banyay, Gregory A, Meyer, Gregory A and Walker, Adam P.** Boston, MA : ASME, 2015. Pressure Vessels and Piping (PVP) Conference.
24. **Takeuchi, K., et al., et al.** *MULTIFLEX: a FORTRAN-IV Computer Program for analyzing thermal-hydraulic-structure system dynamics (WCAP-8709).* Pittsburgh, PA, USA : Westinghouse Electric Company, 1976.
25. **United States Nuclear Regulatory Commission.** Regulatory Guide 1.60, Rev. 2. *Design Response Spectra for Seismic Design of Nuclear Power Plants.* Rockville, MD, USA : United States Nuclear Regulatory Commission, July 2014.
26. **Converse, April and Brady, A Gerald.** *BAP basic strong-motion accelerogram processing software version 1.0.* s.l. : United States Department of the Interior, U.S. Geological Survey, 1992.
27. **Morgan, M G, Henrion, Max and Small, M.** *Uncertainty: A Guide to Dealing with Uncertainty in Quantitative Risk and Policy Analysis.* Cambridge : Cambridge University Press, 1992.
28. *Nonlinear Sensitivity Analysis of Multiparameter Model Systems.* **Cukier, R I, Levine, H B and Shuler, K E.** 1978, Journal of Computational Physics, Vol. 16, pp. 1-42.
29. *Global Sensitivity Analysis – A Computational Implementation of the Fourier Amplitude Sensitivity Test (FAST).* **McRae, G J, Tilden, J W and Seinfeld, J H.** 1980, Computers & Chemical Engineering.
30. *Structural Reliability Analysis using Deterministic Hybrid Simulations and Adaptive Kriging Metamodeling.* **Abbiati, G, et al., et al.** Santiago, Chile : Earthquake Engineering Research Institute, 2017. 16th World Conference on Earthquakes.
31. **Rasmussen, Carl Edward and Williams, Christopher K.I.** *Gaussian Processes for Machine Learning.* Cambridge : MIT Press, 2005.
32. *Design and Analysis of Computer Experiments.* **Sacks, J, et al., et al.** 1989, Statistical Science, Vol. 4, pp. 409-435.
33. **Lataniotis, C, Marelli, S and Sudret, Bruno.** UQLab User Manual – Kriging (Gaussian Process Modelling). *Report UQLab-V1.0-105.* Zurich : ETH-Zurich, 2017.

34. *Reliability analysis using adaptive kriging surrogates with multimodel inference.* **Sundar, V S and Shields, Michael D.** 2018, ASCE-ASME Journal of Risk and Uncertainty in Engineering Systems: Part A Civil Engineering.
35. **Iman, Ronald L, Davenport, James M and Zeigler, Diane K.** *Latin Hypercube Sampling (Program User's Guide).* Albuquerque, NM : Sandia Laboratories, 1980.
36. *A central limit theorem for Latin hypercube sampling with dependence and application to exotic basket option pricing.* **Aistleitner, Christoph, Hofer, Markus and Tichy, Robert.** 7, 2012, International Journal of Theoretical & Applied Finance, Vol. 15.
37. **Loh, Wei-Liem.** *On the Convergence Rate to Normality of Latin Hypercube Sampling U-Statistics.* Statistics, Purdue University. West Lafayette, IN : Purdue University, 1995.
38. *The Generalization of Latin Hypercube Sampling.* **Shields, Michael D and Zhang, J.** 2016, Reliability Engineering & System Safety, Vol. 148, pp. 96-108.
39. *A Comparison of Three Methods for Selecting Values of Input Variables in the Analysis of Output from a Computer Code.* **McKay, M D, Conover, W J and Beckman, R J.** 2, 1979, Technometrics, Vol. 21, pp. 239-245.
40. **Montgomery, Dallas C.** *Design and Analysis of Experiments.* 8. Hoboken : John Wiley & Sons, 2013.
41. **Blevins, Robert D.** *Flow-Induced Vibration.* 2. Malabar : Kreiger, 2001.
42. **Kaizer, Joshua S.** *Fundamental Theory of Scientific Computer Simulation Review.* Mechanical Engineering, University of Maryland. College Park, MD : s.n., 2013. Dissertation. NUREG/KM-0006.
43. **Oberkampf, William L, Pilch, Martin and Trucano, Timothy G.** *Predictive Capability Maturity Model for Computational Modeling and Simulation.* Validation and Uncertainty Quantification. Albuquerque, NM : Sandia National Laboratories, 2007.
44. *Predictive Capability Maturity Assessment with Bayesian Network.* **Lin, Linyu and Dinh, Nam Truc.** Philadelphia, PA : American Nuclear Society Summer Meeting, 2018.

Figure Captions List

Table Caption List